An Ultra-Low Field imaging instrument and analysis of its SNR and scaling properties

B-H. Eom[1], M. S. Cohen[2], I. Hahn[1], and K. I. Penanen[1]

[1]Jet Propulsion Laboratory, California Institute of Technology, Pasadena, CA, United States, [2]Psychiatry, University of California, Los Angeles, Los Angeles, CA, United States

Abstract

With all of its advantages in diagnostic power and extraordinary risk profile, MRI is among the most costly of radiologic methods, and the physical characteristics of the instrument, including its size, weight, SAR, siting restrictions and limited patient space present very real limitations.

The possibility of imaging at very low fields using direct magnetometry has been demonstrated recently and many advantages have been noted. Here we present our work towards the construction of a practical instrument Ultra-Low Field MRI (ULFMRI) for human clinical imaging.

Methods

We designed and built a scaled prototype instrument capitalizing that incorporates several significant novel elements. In our device the sample, which may be up to approximately 10 cm in diameter, is polarized using a pair of air-cooled copper wound electromagnets that can develop a field of up to 0.1T. Our detector coil is an axisymmetric second-order gradiometer sensing coil with 33 mm baseline and 24 mm loop diameter wound on a fused silica former with an 80 μm Nb wire. The gradiometer is aligned symmetrically to the polarization field and achieves 140 dB rejection of the polarization flux. To further reduce the problems of ring-down that result from such coupling, we use broadband, DC coupled electronics for the SQUID readout. We built a three axis gradient set onto 1 meter formers that is used also to create the readout field. A separate set of coils surround the entire apparatus to provide earth field cancellation allowing us to capture signal at 170 μT (7.3 kHz). An untuned excitation coil is used for NMR induction. Though other pulsing sequences are possible, we typically use a 3 dimensional spatial encoding scheme and achieve submillimeter spatial resolution in reasonable imaging times of 8 minutes or less (figure) with acceptable SNR

Discussion

In Figure 1, we show the image noise normalized to the signal intensity. To obtain this data, we took a series of images of a cylindrical phantom. We show the pixel intensity noise in the image as a function of the pixel intensity. Imaging field instabilities would manifest in this graph as enhanced noise at intermediate intensities due to the motion of the phantom boundaries. Signal gain irreproducibility would show as enhanced noise at larger intensities. We observe the pixel intensity noise is nearly independent of the intensity. The horizontal dashed line in the figure indicated the noise level when the imaging fields are turned off and the polarization is not applied. This level is consistent with the intrinsic SQUID noise. Practical acceptance of a new MRI device, even without the limitations discussed above for conventional instruments, will almost certainly require image quality comparable to standard commercial units over the range of applications most typically encountered in the clinic. We therefore studied the problems of device scaling and signal quality. A separate abstract considers the issues of tissue behavior at ultra-low field. Under the assumption that T2 is of the same order as the readout period, in MRI we can model:

$$\frac{SNR}{\text{Voxel}} \propto \frac{\text{flux/voxel}}{\text{noise/voxel}} \sqrt{\text{total sampling time}} \propto \frac{B_p(1-e^{-T_p/T_1})e^{-te/T_2}}{\sqrt{S \times BW}} \frac{N_G F_G}{D_G} \sqrt{T_t},$$

where S is the noise power per bandwidth, T_P is the polarization time, te is the MRI echo time, BW is the bandwidth per pixel, N_G is the number of turns of the receiver coil, F_G is the geometrical factor describing the distance separating the sample from the detector, D_G is the loop diameter of the gradiometer and T_t is the total sampling time. The measured SNR of our device at a distance of 2.3 cm from the gradiometer is approximately 10 with an imaging time of 1 minute/slice using a pure water phantom. Typical human neuroimaging devices show an SNR of about 30 over a cylindrical field of view of 24 cm radius and 20 cm length with a similar voxel volume. Further, the acquisition must be completed within a clinically acceptable imaging time of about 30 minutes. In conventional high field MRI devices, the bandwidth is determined ultimately by the observed transverse relaxation time, T2*, which itself is limited principally by field homogeneity. Bandwidths of 16 kHz to 50 kHz are typically employed to mitigate this effect and distortions from chemical shift. By contrast, with the T2* we measured here we can use bandwidths of 1 kHz or less without suffering unacceptable apodization blurring. The magnitude of the polarization field, B_p, is limited in pre-polarization experiments such as ours, by the need to avoid unacceptable magneto-stimulation as the field is cycled rapidly down to the measurement field. We anticipate that 0.2 Tesla will be a practical limit more than two fold higher than our current operating point.

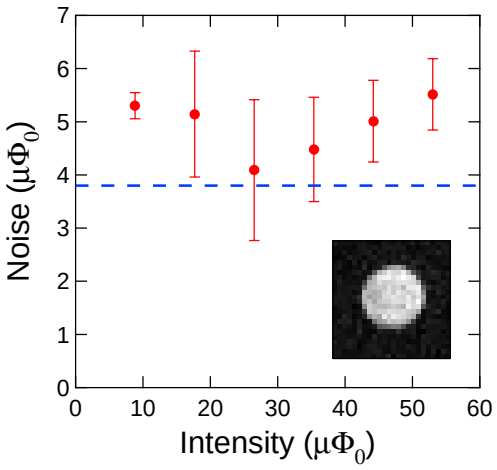

Figure 1. Per-pixel magnetic flux noise vs. flux. The dashed line indicates noise with no imaging fields. Inset: Phantom image (13 mm diameter) used for noise evaluation.

An important difference between ULFMRI and MRI as typically practiced is that the achievable SNR in the megahertz range quickly becomes body noise limited. This is not the case at 7.5 kHz and indeed, the body noise is unmeasurable with our detectors. Instead, the SNR is dominated mainly by the low noise floor of our commercial SQUID devices as shown in Fig.1. The technology of the SQUID, however, has ample headroom for improvement and, indeed we anticipate substantially reduced noise with our next generation of home built detectors.

Although the magnet itself is the most expensive single component of standard MRI instruments (and is essentially eliminated in our designs), non-renewable cryogens are placing increasing pressure on the operational costs and the prices have risen dramatically. MRI is an enormous factor in this commodity, accounting for about 25% of the market (source: F. Scott Murray, VP and general manager of Philips' magnet group). Though our prototype is immersed in a He dewar, the relatively small thermal mass of the superconducting components of ULFMRI instruments maybe cryocooled directly with only modest energy costs. In our own lab, we are presently fabricating a human MRI device that is expected to weigh less than 550 kg with a footprint of 1 m^2 and cryogen-free operation. The potential of successful ultra-low field imaging devices include an order of magnitude reduction in end-user cost, the ability to operate units at very low power, the availability of imaging within the operating theater that does not interfere with normal patient access, the opportunity to deliver imaging to the field in emergency situations and a host of other advantages.